

ORIGINAL ARTICLE

Linearity Can Account for the Similarity Among Conventional, Frequency-Doubling, and Gabor-Based Perimetric Tests in the Glaucomatous Macula

HAO SUN, PhD, MITCHELL W. DUL, OD, MS, FAAO, and WILLIAM H. SWANSON, PhD, FAAO

Glaucoma Institute (HS, MWD, WHS), Department of Biological Sciences (HS), and Department of Clinical Sciences (MWD, WHS), State University of New York, State College of Optometry, New York, New York

ABSTRACT

Purposes. The purposes of this study are to compare macular perimetric sensitivities for conventional size III, frequency-doubling, and Gabor stimuli in terms of Weber contrast and to provide a theoretical interpretation of the results.

Methods. Twenty-two patients with glaucoma performed four perimetric tests: a conventional Swedish Interactive Threshold Algorithm (SITA) 10-2 test with Goldmann size III stimuli, two frequency-doubling tests (FDT 10-2, FDT Macula) with counterphase-modulated grating stimuli, and a laboratory-designed test with Gabor stimuli. Perimetric sensitivities were converted to the reciprocal of Weber contrast and sensitivities from different tests were compared using the Bland-Altman method. Effects of ganglion cell loss on perimetric sensitivities were then simulated with a two-stage neural model.

Results. The average perimetric loss was similar for all stimuli until advanced stages of ganglion cell loss, in which perimetric loss tended to be greater for size III stimuli than for frequency-doubling and Gabor stimuli. Comparison of the experimental data and model simulation suggests that, in the macula, linear relations between ganglion cell loss and perimetric sensitivity loss hold for all three stimuli.

Conclusions. Linear relations between perimetric loss and ganglion cell loss for all three stimuli can account for the similarity in perimetric loss until advanced stages. The results do not support the hypothesis that redundancy for frequency-doubling stimuli is lower than redundancy for size III stimuli.

(Optom Vis Sci 2006;83:E455–E465)

Key Words: perimetry, glaucoma, macula, SITA 10-2, frequency-doubling, Gabor

Conventional automated perimetry is widely used in diagnosis of glaucoma and in evaluating effects of glaucoma treatment. The most commonly performed conventional perimetric test uses a small luminance increment stimulus (Goldmann size III, 0.43° diameter) superimposed on a uniform white background. With this stimulus, test–retest variability is high in areas with decreased sensitivity,^{1–3} which makes it difficult to detect progression of visual field loss. Test–retest variability in these areas can be reduced^{4,5} by using a larger stimulus (Goldmann size V, 1.72° diameter), but increasing stimulus size can decrease the depth of defect and the ability to detect visual field change.^{5–7} An alternative is to use cathode ray tube (CRT)-based perimetric tests, which use large sinusoidal stimuli such as counterphase-modulated

gratings used in frequency-doubling perimetry^{8,9} or Gabor stimuli (sinusoidal gratings with Gaussian envelopes) used in contrast sensitivity perimetry.¹⁰ A recent study has shown that test–retest variability is less dependent on depth of defect for frequency-doubling stimuli than for size III stimuli, and that until advanced stages of visual field loss, there is a relatively consistent relation between sensitivities for frequency-doubling stimuli and sensitivities for size III stimuli.³

It is still not well understood how to quantitatively relate perimetric sensitivities for Goldmann size III stimuli to those for frequency-doubling gratings. The two stimuli have different spatial and temporal configurations; one is a small luminance increment that is pulsed on briefly and the other is a low spatial frequency

grating that is counterphase-modulated at a high temporal frequency. The different stimulus configurations may lead to different responses from the retinal and cortical cells and hence different perimetric sensitivities. The printouts for the two types of perimeters are not directly comparable because each machine uses a different definition of sensitivity. Most of the previous comparison studies have taken an empiric approach; the response variability and depth of defect have been compared with arbitrary units⁸ such as in terms of the dynamic ranges of the devices⁹ or in terms of probability values based on normative data.¹¹ Without a theoretical justification for choice of units, it is difficult to make quantitative comparisons of defect depth and test variability. For example, a defect of -10 dB on the Humphrey Field Analyzer means 90% loss, whereas on the Humphrey Matrix it means 68% loss.

In this study, we provide a theoretical basis for comparing perimetric sensitivities with Goldmann size III and frequency-doubling stimuli in terms of Weber contrast.³ Perimetric sensitivities for different stimuli were compared directly without requiring a normative database. We also included a Gabor stimulus, which is similar to the frequency-doubling grating in spatial configuration and similar to the size III stimulus in temporal configuration. Our data were consistent with similar sensitivity loss for all three stimuli despite the different spatial and temporal configurations. To interpret the data, we used a two-stage neural model¹² to simulate perimetric sensitivities for size III, frequency-doubling and Gabor stimuli. A comparison of model simulations with experimental data suggests that experimental data can be explained if linear relations between perimetric sensitivity loss (perimetric sensitivity is defined as the reciprocal of perimetric threshold) and ganglion

cell loss hold for all three stimuli until advanced stages of ganglion cell loss.

METHODS

Subjects

Twenty-two patients with early to advanced glaucoma were recruited (see Table 1 for age and clinical characteristics). All patients have previously been diagnosed by an experienced clinician (MWD). Patients were required to have visual acuity of 20/30 or better, refractive errors of less than ± 6 D of sphere and 3 D of cylinder, clear ocular media, no systemic disorder or medication known to affect visual function, and no other eye disease. This study followed the tenets of the Declaration of Helsinki. Written informed consent was obtained from all observers after the nature and possible consequences of the study were explained. This research was approved by the Institutional Review Board of the SUNY State College of Optometry. Financial compensation was given to each patient for their travel expenses and time.

Apparatus and Stimulus

Four perimetric tests (Swedish Interactive Threshold Algorithm [SITA] 10-2, FDT 10-2, FDT Macula, and Gabor) were performed using three testing stations: a Humphrey Field Analyzer II (Carl Zeiss Meditec, Dublin, CA), a Humphrey Matrix (Zeiss-Humphrey, Welch Allyn FDT Visual Field Instrument/Welch Allyn, Skaneateles, NY), and a VSG-controlled (VSG 2/5; Cam-

TABLE 1.

Patient information: age, diagnosis, refractive error, visual acuity, Pelli-Robson contrast sensitivity, MD for Swedish Interactive Threshold Algorithm (SITA) 24-2 and 10-2, and partial means for locations that were used in the Bland-Altman analysis in Figure 5A and PSD for SITA 24-2 and 10-2

Age	Diagnosis	Refraction	Acuity	Pelli-Robson	24-2, 10-2, partial MD (dB)	24-2, 10-2 PSD
49	POAG	-1.5	20/20	1.50	-26.45/-23.11/-11.15	8.92/13.17
67	POAG	0.0-1.0 × 60	20/25	1.30	-30.7/-18.93/-10.82	5.15/11.74
68	POAG	-2.75	20/20	1.50	-12.96/-13.46/-5.17	12.89/15.46
44	POAG	+0.75	20/20	0.95	-14.78/-10.19/-3.53	11.91/14.31
65	POAG	0.0	20/30	1.50	-14.55/-10.8/-8.88	9.84/7.5
80	POAG	+1.5	20/25	1.65	-3.51/-9.66/-3.47	6.84/13.7
67	POAG	+1.25-1.25 × 0	20/16	1.55	-11.54/-9.2/-4.56	8.37/7.42
70	NTG	+2.5-0.75 × 90	20/25	1.45	-5.41/-4.33/-4.33	4.59/6.19
53	POAG	-5.5-0.5 × 175	20/30	1.40	-5.13/-3.45/-3.38	3.17/2.94
67	POAG	+1.5-1.25 × 20	20/30	1.35	-11.52/-3.2/-1.94	8.17/2.03
71	CMG	0.0-1.0 × 135	20/30	1.45	-8.21/-3.05/-1.74	5.44/2.84
68	CMG	2.75-1.0 × 100	20/30	1.35	-9.94/-3.05/-0.56	8.63/4.71
64	POAG	+0.25	20/20	1.50	-5.79/-2.93/-1.75	2.33/2.05
65	POAG	0.0	20/16	1.45	-2.17/-2.59/-2.19	2.29/1.82
59	POAG	+2.5-1.0 × 80	20/16	1.65	-8.33/-2.59/-1	4.8/2.75
57	POAG	0.0	20/20	1.50	-3.15/-1.42/-3.06	5.16/2.85
70	POAG	+2.5-0.75 × 95	20/20	1.50	-12.7/-1.41/-1.75	11.68/1.33
56	POAG	-0.25-1.0 × 110	20/16	1.80	-1.13/-1/-0.81	2.11/1.07
72	POAG	0.0	20/20	1.65	-3.12/-0.54/0.19	2.1/2.29
62	POAG	+1.25-1.0 × 90	20/30	1.55	0.24/-0.16/-0.31	1.81/1.25
58	POAG	0.0	20/20	1.65	-2.9/-0.14/-0.13	3.57/1.54
62	POAG	+0.75-0.5 × 70	20/20	1.65	-2.47/0.7/0.69	1.41/1.17

PSD, pattern standard deviation; POAG, primary open-angle glaucoma; NTG, normal tension glaucoma.

bridge Research Systems, Kent, U.K.) CRT-based system. The first two were commercially available clinical devices, and the third one was designed in our laboratory.

The SITA 10-2 test was performed on the Humphrey Field Analyzer. The stimulus (Goldmann size III) was a 0.43° diameter circular luminance increment (Fig. 1A). It was presented as a 200-ms rectangular pulse. The 68 test locations formed a 2°-offset grid that covered the central ±10° visual field. The grid was symmetric to both horizontal and vertical meridian with no locations falling on the meridian. The maximum and minimum luminances of the stimulus that can be generated by the apparatus were 3183 and 0.025 cd/m². The background luminance was 10 cd/m². Sensitivities given in the Humphrey Field Analyzer printout were expressed as the relative attenuation from the maximal stimulus luminance in decibel units, with 10 dB per log unit and 0 and 51 dB corresponding to the maximum and minimum stimulus luminances, respectively.

The FDT 10-2 and FDT Macula tests were performed on the Humphrey Matrix. For both tests, the stimulus was a 0.5 cycle per degree (cpd) grating patch (2° × 2°), which was temporally counterphase-modulated at 12 Hz (Fig. 1B). At these spatial and temporal frequencies, the stimulus is not likely to give frequency-doubling percept.¹³ The stimulus was presented for a total of 720 ms: 400 ms for the maximum contrast and 160 ms each for linear ramp-on and ramp-off. The background luminance was 90 cd/m² (calibrated with a Minolta LS-100 Lumi-

nance Meter; Konica Minolta Sensing, Sakai, Osaka, Japan). The spatial and temporal average luminance of the test patch was the same as that of the background. The FDT Macula test included 16 test locations in the central ±5° of visual field. The FDT 10-2 test included 44 test locations in the central ±10° of visual field, of which 16 locations in the central ±5° were the same as those in the FDT Macula and SITA 10-2 tests and the other locations between ±5° and ±10° were not the same as those in the SITA 10-2 test. Sensitivities given in the Humphrey Matrix printout were expressed as the reciprocal of Michelson contrast in decibel units with 20 dB per log unit and 0 dB representing the maximum contrast (100%).

The Gabor test was performed on the VSG-controlled CRT (SONY Trinitron GDM-F500, 150-Hz frame rate) system. The stimulus was a Gabor sine with peak spatial frequency of 1.0 cpd and a spatial bandwidth at half-height of 0.7 octave (Fig. 1C). It was presented for 600 ms with a Gaussian temporal envelope (100-ms time constant). The average luminance of the stimulus and the background luminance were both 50 cd/m². There were eight test locations, four at ±3°, ±3° and four at ±9°, ±9°. The four locations at ±3°, ±3° were the same as those of the FDT and SITA 10-2 tests. Sensitivities given in the Gabor test printouts were expressed as the reciprocal of Michelson contrast in logarithmic units, with 0.0 representing 100% contrast and 2.0 representing 1% contrast.

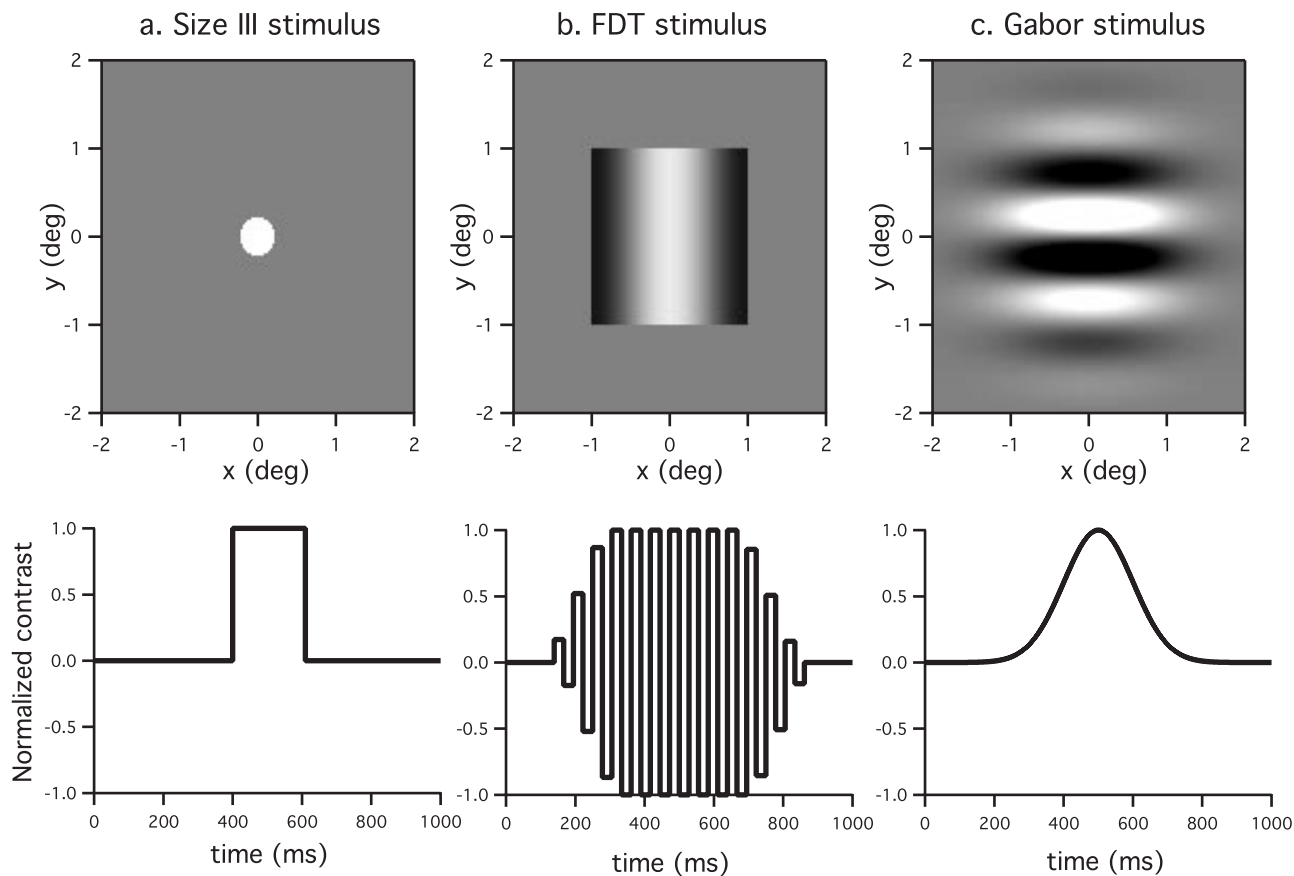


FIGURE 1.

The spatial (top row) and temporal (bottom row) configurations for the size III stimulus of (a) the Humphrey Field Analyzer, (b) the frequency-doubling stimulus of the Humphrey Matrix, and (c) the Gabor stimulus of the cathode ray tube system.

Procedures

Different algorithms were used in each apparatus to measure thresholds. In the Humphrey Field Analyzer, thresholds were assessed with the SITA procedure.¹⁴ In the Humphrey Matrix, thresholds were assessed using a ZEST procedure.¹⁵ Both procedures assumed probability density functions for the threshold value. In the VSG-controlled CRT system, sensitivities were measured with a staircase procedure in which the equivalent sensitivity of a stimulus (i.e., the reciprocal of stimulus contrast) was varied in linear steps. The initial step size was 0.5, and it was reduced to 0.25 after the first reversal and to 0.125 after the second reversal. Each staircase was terminated after six reversals, and the threshold was calculated as the average of the last four reversals. Eight staircases (one for each stimulus location) were randomly interleaved.

All four perimetric tests were performed in a single visit with the same eye with breaks between each test. The order of perimetric tests was counterbalanced. Before the perimetric tests, patients were tested with a logarithmically scaled (logarithm of the minimum angle of resolution) visual acuity chart (Lighthouse Low Vision Products “ETDRS” Cat No 2170; Precision Vision, La Salle, IL) and a Pelli-Robson contrast sensitivity chart (Clement Clarke International Ltd., Harlow, Essex, U.K.).

Data Analysis

As a preliminary analysis, we assessed whether SITA 10-2 and FDT 10-2 tests were concordant by clinical standards. Machine printouts were compared by one of the authors (MWD) and were assessed in terms of total sensitivity deviation and probability values from the machine database (MD and PSD). For each patient, concordance between the SITA 10-2 and FDT 10-2 tests was evaluated based on whether the same hemifield and the same quadrant had the lowest total sensitivity across all the locations in that hemifield or quadrant.

The main statistical analyses did not rely on machine databases or on assessments of the spatial patterns of visual fields. We did a pointwise comparison of sensitivities obtained with two tests using the Bland-Altman method.¹⁶ For each location and each patient, we plotted the difference in the two sensitivities as a function of their mean. Linear regression was used to assess dependence of the difference on the mean and to generate 95% confidence limits for the differences. We first compared sensitivities for the SITA 10-2 and FDT 10-2 tests, which used two different stimuli. Then we compared sensitivities for the FDT 10-2 and Gabor tests, both of which used sinusoidal stimuli. Finally, we compared sensitivities for the FDT 10-2 and FDT Macula tests, both of which used the same stimulus. For the comparison between the two FDT tests, we also performed an F test on the standard deviation of the sensitivity differences to evaluate whether the variation was greater across different stimuli than across the same stimuli.

All comparisons were restricted to test locations that were shared by both tests in the central $\pm 5^\circ$ of visual field. This yielded a total of 88 locations (four locations per eye) for comparisons involving the Gabor test and 352 locations (16 locations per eye) for other comparisons. Because different locations cannot be considered independent when they are tested from the same person, we made conservative estimates of statistical significance by determining the

degrees of freedom based on the number of patients. When a statistical test found no significant difference, we repeated it with the degrees of freedom based on the total number of locations to determine whether the conservative estimates were too limited in statistical power. We set the significance level to $p < 0.01$ to take into account the total number of statistical tests.

The Bland-Altman method was developed for comparison of two methods of measurement. The examples given in their original paper¹⁶ were for devices that gave results in the same units. For perimetry, there have been no standard units. To provide a common unit, we expressed all sensitivities as the reciprocal of Weber contrast (in logarithmic units, see Appendix, available at <http://www.optivisci.com>). For the Gabor test, sensitivity remained the same. To convert sensitivity for the SITA test, we first subtracted 25 from the Humphrey Field Analyzer printout and then divided the difference by 10. To convert sensitivity for the FDT tests, we divided the Humphrey Matrix printout by 20. For FDT and Gabor tests, the maximum stimulus luminance corresponds to 0.0 log contrast sensitivity, whereas for the SITA 10-2 test, it corresponds to -2.5 log contrast sensitivity. The apparatus dynamic range, defined as the difference between the mean sensitivity of control observers and the minimum sensitivity that can be tested on the machine, is twice as large for Humphrey Field Analyzer than for the Humphrey Matrix and the laboratory-designed testing station. This difference in apparatus dynamic range is a potential source of artifact for regression analysis. Therefore, in the primary Bland-Altman analysis, we excluded 19 locations where sensitivity estimates were 0 or lower than 0 dB (in the machine printout) for one or both tests and 14 locations where mean sensitivities were below 0.0 log unit. In the secondary analysis, we assessed relative sensitivities at these excluded locations.

Model Simulation

Why is the perimetric performance for the three stimuli similar although their spatial and temporal properties are different? What does this tell us about the relation between ganglion cell loss and perimetric sensitivity? Electrophysiological and anatomic studies have suggested a linear relation between ganglion cell loss and perimetric sensitivity to size III stimuli.^{17–20} If the linear relation extends to the frequency-doubling and Gabor stimuli, this could explain our results. To explore this hypothesis, we used a two-stage neural model¹² to simulate perimetric sensitivities for size III, frequency-doubling, and Gabor stimuli.

In the first stage of the neural model, the stimulus was centered on an array of retinal ganglion cells and the response of each ganglion cell was computed by multiplying the 2D stimulus with the cell's receptive field. In the second stage, ganglion cell responses were pooled by an array of spatial filters representing populations of cortical neurons (Fig. 2). The response of each filter was computed by multiplying the ganglion cell responses with a weighting factor based on the filter's spatial profile, with excitatory regions having positive weights and inhibitory regions having negative weights. The weighted responses of the ganglion cells were summed to produce the response of the spatial filter. Internal noise was added only to the cortical filter response, because, for cortical neurons, internal noise is the primary factor in the output noise even in the presence of high input noise.^{21,22} Psychophysical sen-

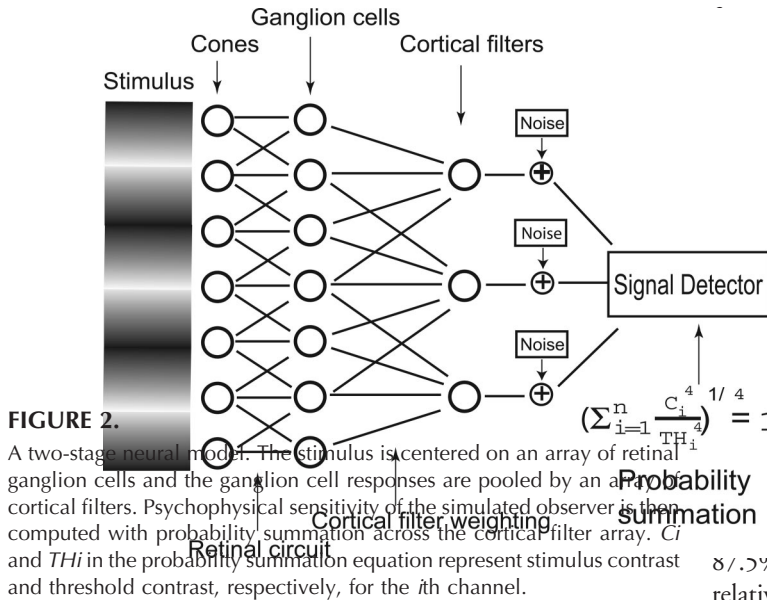


FIGURE 2. A two-stage neural model. The stimulus is centered on an array of retinal ganglion cells and the ganglion cell responses are pooled by an array of cortical filters. Psychophysical sensitivity of the simulated observer is then computed with probability summation across the cortical filter array. C_i and TH_i in the probability summation equation represent stimulus contrast and threshold contrast, respectively, for the i th channel.

sensitivity was computed by probability summation as described by Pelli²³ with an exponent of 4.^{24–27}

For the first stage, the receptive field of a ganglion cell was simulated with a difference of two Gaussian functions. Each ganglion cell array was specified by four parameters: Gaussian radii of ganglion cell receptive field center and surround, ratio of peak sensitivity for center and surround Gaussian, and spacing between ganglion cells (Table 2). Based on reports of primate ganglion cell receptive fields²⁸ and human ganglion cell density,²⁹ we chose three sets of parameters to represent three types of ganglion cell arrays: macular, dense, and sparse. The macular array had the highest density of ganglion cells and the smallest receptive fields and considerable overlap of receptive field centers. The dense array had intermediate ganglion cell density with similar overlap of receptive field centers as the macular array. The sparse array had the largest receptive fields and the lowest density with least overlap of receptive field centers. The macular and dense arrays approximated the density of mixed magnocellular and parvocellular cells at the fovea and at 9° eccentricity,²⁹ whereas the sparse array approximated the density of only magnocellular cells at 9° eccentricity.

For the second stage, the receptive field of a cortical filter was simulated using derivatives of Gaussians, either edge detectors (D1) or narrow-band filters in sine (D5) or cosine (D6) phase, with an orthogonal Gaussian envelope.¹² The cortical filter was specified by five parameters: phase (sine or cosine), peak spatial frequency, spatial bandwidth, peak orientation, and orientation bandwidth. Each filter in an array had the same phase, spatial

frequency, spatial bandwidth, and orientation bandwidth but the orientation varied systematically from 0° to 315° in steps of 45°. We used filter arrays in both sine and cosine phase with peak frequency varied from 0.25 to 4.0 cpd in octave steps, bandwidths varied from 1.0 to 2.6 octaves, and orientation bandwidths varied from 14° to nonoriented. Filter spacing was defined by ganglion cell spacing with one cortical filter centered on one ganglion cell.

Perimetric sensitivity of the simulated observers was computed for each stimulus and for seven levels of ganglion cell loss. The three stimuli, a 0.43° diameter circle, a 0.5-cpd grating (2° × 2°), and a 1.5-cpd Gabor sine (0.7-octave bandwidth), are referred to as size III, size II, and size I stimuli although the model does not take into account their temporal configurations. For each ganglion cell array, perimetric sensitivity was computed for seven levels of ganglion cell loss, either as a result of cell loss or reduction of sensitivity because of dysfunction, was simulated by randomly removing cells to produce 25%, 50%, 75%, 87.5%, 93.75%, 96.87%, and 98.44% cell loss (corresponding to relative ganglion cell loss from -0.1 to -1.8 log unit). The size III stimulus was relatively small compared with the sparse ganglion cell spacing, and small changes in stimulus position could cause significant changes in sensitivity, especially when the ganglion cell loss is severe; therefore, the perimetric sensitivity was obtained by averaging sensitivities at a grid of 13 different stimulus locations centered within a 2° circle. The Gabor and FDT stimuli were much larger and stimulus location had little effect on sensitivity, so perimetric sensitivity was obtained only for a single location.

RESULTS
Clinical Assessment and Case Examples

Clinical assessment of visual field concordance showed good agreement between SITA 10-2 and FDT 10-2 tests. Printouts were concordant for 20 of 22 (90%) patients in terms of which hemifield had lower total sensitivity. For 18 of 22 (82%) patients, there was also agreement in terms of which quadrant had the lowest total sensitivity. The two patients for whom the fields were not concordant had little sensitivity loss (SITA 10-2 MD ≥ -3 dB, PSD ≤ 3 dB).

Figure 3 shows gray scale plots for SITA 10-2, FDT 10-2, FDT Macula, and Gabor tests for two patients. Data from the two patients illustrate two different patterns of result. For patient no. 1, at two locations (-1,3 and -3,3), FDT printouts were 23 and 27 dB, whereas the SITA 10-2 printouts were 0 dB. For patient no. 2, at three locations (-1,3, -1,1, and 1,3), the SITA 10-2 printouts were between 0 and 6 dB, whereas the FDT 10-2 printouts were

TABLE 2. Parameters used in the first stage of model simulation: the space constants for ganglion cell’s receptive field center and surround and their weights and the spacing between cells^a

Condition	Center radii r_c (°)	Surround radii r_s (°)	Peak sensitivity ratio: center to surround k_c / k_s	Spacing (°)
Macular	0.03	0.18	163.86	0.015
Dense	0.07	0.54	129.67	0.036
Sparse	0.18	1.19	57.5	0.16

^aWe used median values for receptive field parameters from Croner and Kaplan²⁸ for parvocellular cells at 0° to 5° and 10° to 20° (macular and dense conditions) and for magnocellular cells at 10° to 20° eccentricity (sparse condition).

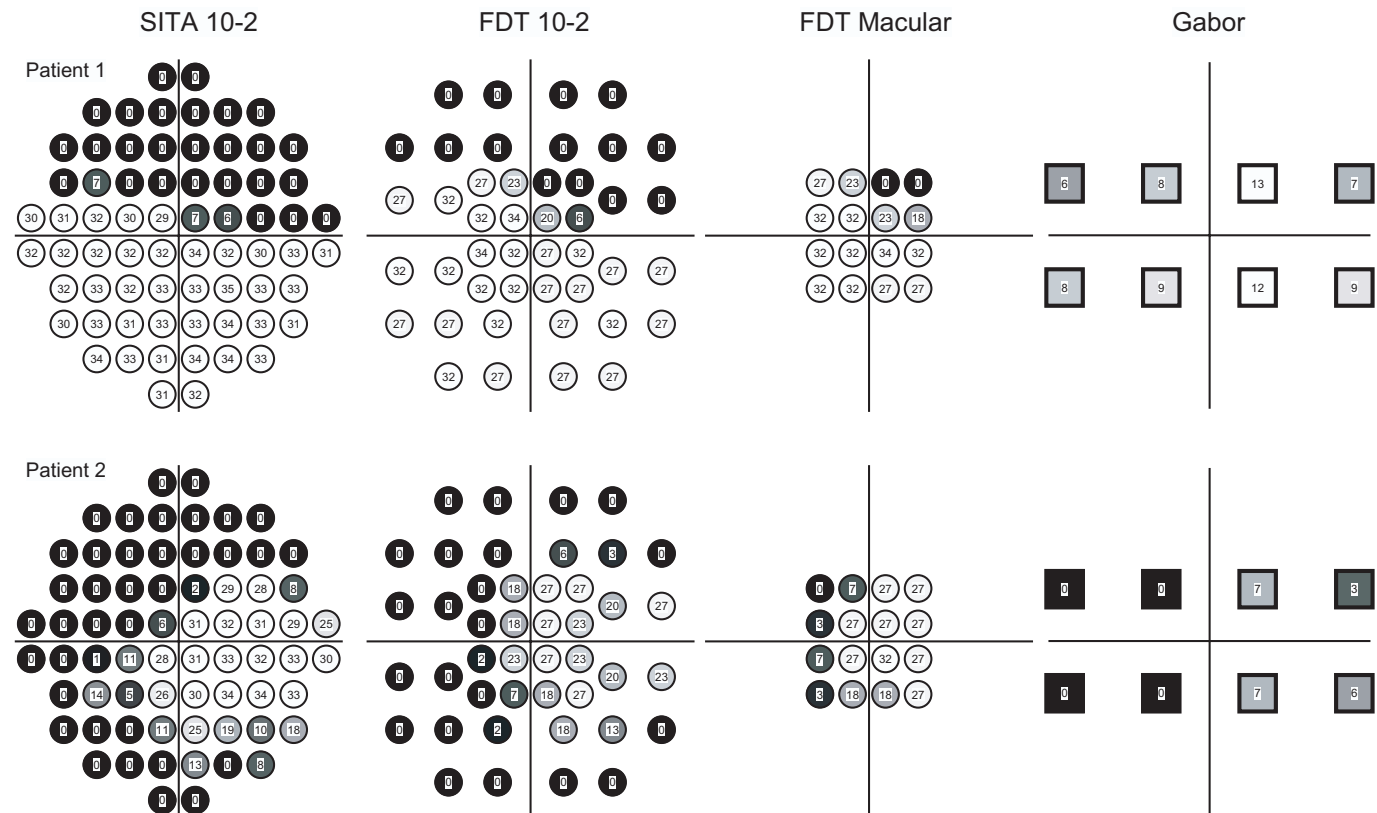


FIGURE 3. Gray-scale plots for SITA 10-2, FDT 10-2, FDT Macula, and Gabor tests for two patients. Two patients show different result patterns. For patient no. 1, at two locations (-1,3 and -3,3), FDT printouts were 23 and 27 dB, whereas the SITA 10-2 printouts were 0 dB. For patient no. 2, at three locations (-1,3, -1,1, and 1, 3), the SITA 10-2 printouts were between 0 and 6 dB, whereas the FDT 10-2 printouts were between 18 and 27 dB, but at two other locations (-1,-3 and -3,-1), the SITA 10-2 printouts were 26 and 11 dB, whereas the corresponding FDT 10-2 printouts were only 7 and 2 dB.

between 18 and 27 dB, but at two other locations (-1,-3 and -3,-1), the SITA 10-2 printouts were 26 and 11 dB, whereas the corresponding FDT 10-2 printouts were only 7 and 2 dB. For both patients, the patterns of FDT 10-2 and FDT Macula results were similar in the central ±5° of visual field.

Bland-Altman Analysis

Figure 4 shows scatterplots for three sets of comparisons: SITA 10-2 versus FDT 10-2, Gabor versus FDT 10-2, and FDT 10-2 versus FDT Macula. Data points that fall on the x- and y-axes

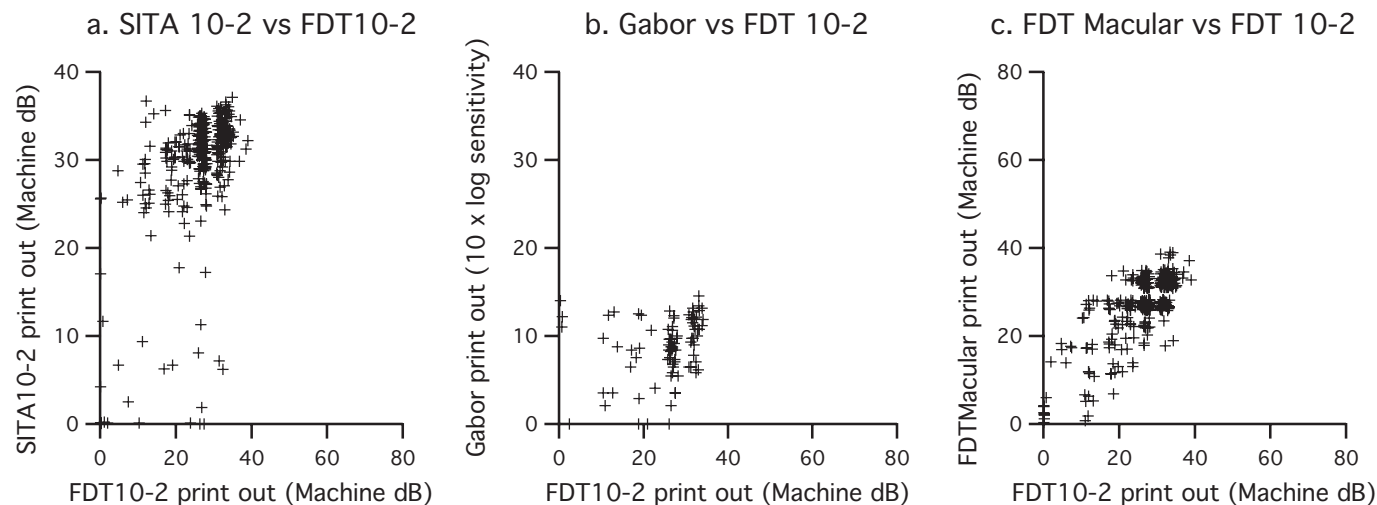


FIGURE 4. Scatter plots for (a) SITA 10-2 versus FDT 10-2 tests, (b) Gabor versus FDT 10-2 tests, and (c) FDT Macula versus FDT 10-2 tests. Data for the SITA 10-2 and two FDT tests are in decibel units as defined by the machines. Data for the Gabor test are in one tenth of log contrast sensitivity units. The ranges of all axes are chosen to cover 4 log units of contrast sensitivity.

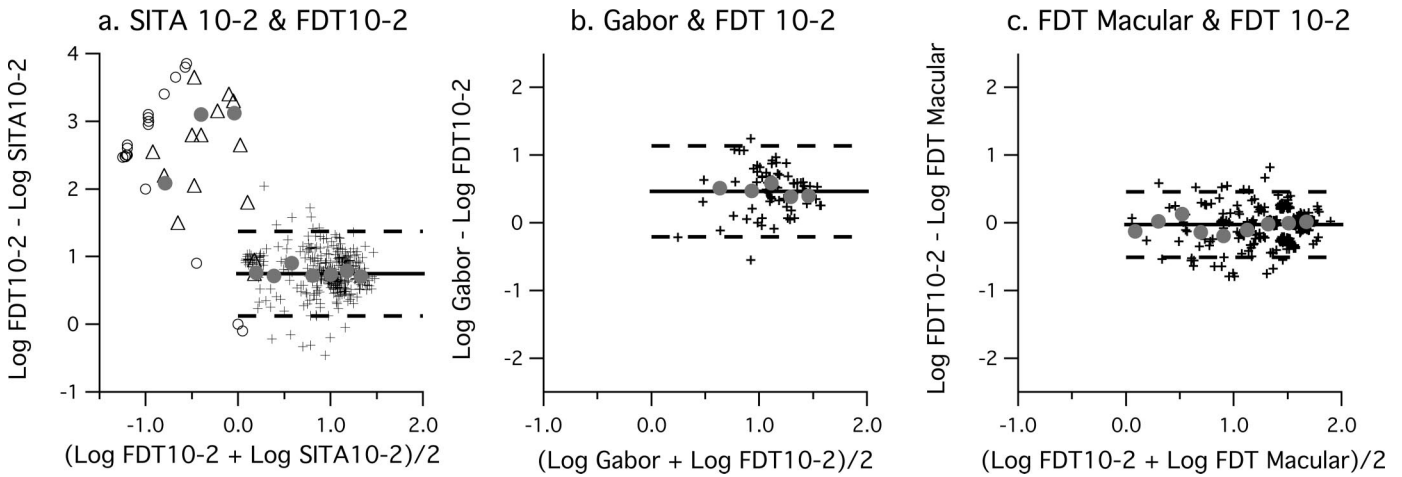


FIGURE 5.

Statistical comparison of (a) SITA 10-2 and FDT 10-2 tests, (b) FDT 10-2 and Gabor tests, and (c) FDT 10-2 and FDT Macula tests. Each cross represents one test location from one patient. The x and y coordinates of each point were varied randomly by a small offset to reveal overlapping data points. Solid circles show means for data grouped into 0.2 log unit bins. The solid line shows the mean difference and the dashed lines bracket the 95% confidence interval. In plot (A), open circles show data points where either one or both thresholds cannot be measured, and open triangles show data points with mean sensitivities lower than 0.0 log unit. These data points are not included in the primary statistical analysis.

represent locations where either of the thresholds could not be measured. Data for the SITA 10-2 and two FDT tests are plotted in decibel units as defined by the Humphrey Field Analyzer and the Humphrey Matrix, respectively. Data for Gabor test are plotted in units of one tenth of log contrast sensitivity. To view overlapping data points, we jittered data for SITA 10-2 and FDT tests by up to 1.25 dB.

Figure 5 shows Bland-Altman plots for the three sets of comparisons shown in Figure 4. Thresholds that are smaller than 0 dB (machine units) were treated as 0. All data were converted into log contrast sensitivity units as described in “Data Analysis.” In the primary comparison of SITA 10-2 versus FDT 10-2, we excluded 19 data points where thresholds were equal or smaller than 0 and 14 data points in which the mean sensitivity (x-axis in Bland-Altman plot) was lower than 0.0 log unit. Statistical assessment of sensitivities at individual locations found that FDT 10-2 sensitivities were higher than SITA 10-2 sensitivities by an average of 0.75 ± 0.31 log unit (Fig. 4A) and were higher than the Gabor sensitivities by an average of 0.46 ± 0.34 log unit (Fig. 4B). For both comparisons, the difference did not vary systematically with sensitivity ($r^2 \leq 0.001$, $p > 0.5$, for df based on both total number of patients and locations) and the width of the 95% confidence limits was approximately 1.0 log unit.

The Bland-Altman comparison for the FDT 10-2 and FDT Macula tests is shown in Figure 5C. On average, the two FDT tests showed very similar sensitivity with a mean difference of 0.03 ± 0.24 log unit and no dependence of the difference on sensitivity ($r^2 \leq 0.01$, $p > 0.1$, for df based on both total numbers of patients and locations). The standard deviation for the sensitivity differences was smaller between the two FDT tests than between FDT and size III tests or between FDT and Gabor tests ($F > 1.66$, $p < 0.01$, for df based on total number of locations). This suggests that the test variation across different stimuli is slightly greater than across same stimuli. If we assume similar test variation for the FDT 10-2 and FDT Macula tests, we can assess the standard deviation for each

FDT test based on the standard deviation between the two FDT tests. This gives an estimated standard deviation of 0.17 log unit, which is consistent with the 8 dB (Humphrey Matrix unit) 90% test–retest intervals found by Artes et al. for the FDT 24 to 2 test.³

Bland-Altman analysis shown in Figure 5 is based one measure with each technique. Does the variability inherent in each technique limit the usefulness of the Bland-Altman analysis? To address this question, we first grouped the data into several bins based on the mean sensitivity and calculated the average of each bin. For all three pairs of Bland-Altman comparisons, the average of each bin was very similar to the overall mean. We also computed the global indices for each individual observer using the geometric mean of the perimetric sensitivities at different locations and repeated the Bland-Altman analysis using each observer’s global indices. The sensitivity difference between the two FDT tests had a variability of 0.14 when computed with global indices compared with 0.24 when computed with individual points; the sensitivity difference between the FDT 10-2 and SITA 10-2 tests had a vari-

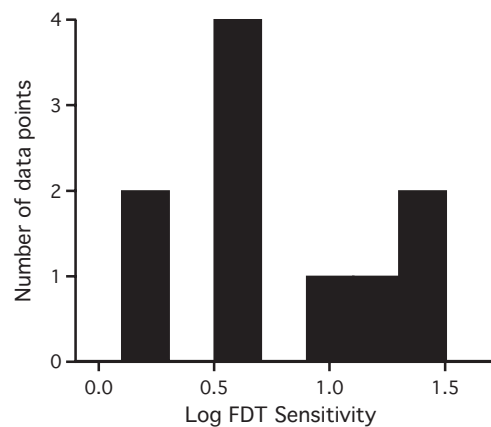


FIGURE 6.

Distribution of FDT 10-2 sensitivities for the 10 locations where thresholds could be measured for FDT 10-2 but not for SITA 10-2.

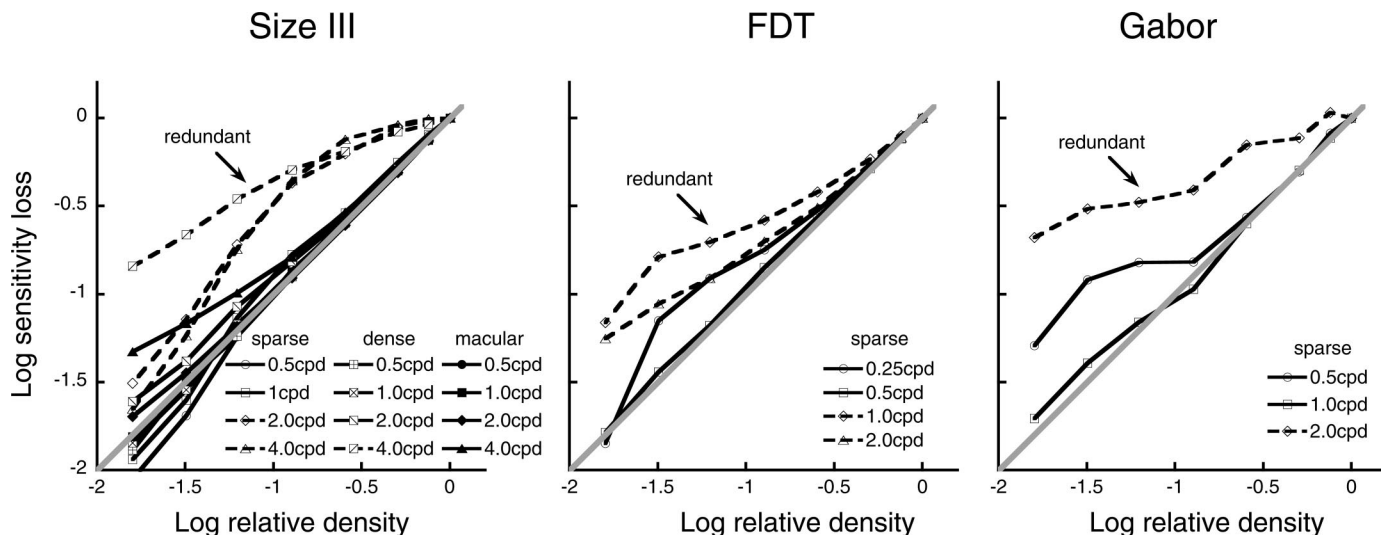


FIGURE 7. Model simulation of perimetry loss as a function of ganglion cell loss for size III, FDT, and Gabor stimuli. Different symbols represent simulation results for macular, dense, sparse ganglion cell arrays with D5 cortical filters of different peak spatial frequencies. For FDT grating and Gabor stimuli, ganglion cell spacing has little effect on the results and only simulation results with the sparse ganglion cell array are shown.

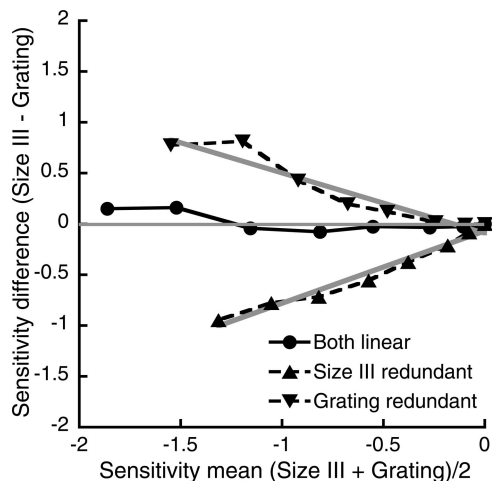


FIGURE 8. Comparison of simulated perimetry sensitivities for size III and FDT stimuli. Circles represent conditions in which linearity holds for both stimuli. The triangles represent conditions in which one stimulus shows redundancy and the other shows linearity.

ability of 0.26 when computed with global indices compared with 0.31 when computed with individual points. Using global indices significantly reduced test variability as would be expected, but it had less effect on variability between SITA 10-2 and FDT 10-2 tests. This suggests that variability inherent in each technique does not affect the usefulness of the Bland-Altman analysis in our study.

We further examined the 33 data points that were excluded from the primary SITA 10-2 and FDT 10-2 comparison. There were five data points where sensitivity could not be measured for both SITA 10-2 and FDT 10-2, 10 data points where only SITA 10-2 sensitivity could not be measured, and 4 data points where only FDT 10-2 sensitivities could not be measured (SITA 10-2 sensitivity was: 0.1, 0, 0.9, 2.0 log unit). Figure 6 shows the distribution of FDT 10-2 sensitivities for the 10 locations where sensitivity could be measured for FDT 10-2 but not for SITA 10-2. For

the remaining 14 data points where both sensitivities were measurable but the mean was lower than 0.0 log unit, the difference between FDT and SITA sensitivities averaged 2.68 ± 0.64 log unit.

Model Simulation

We used a two-stage neural model to simulate perimetric sensitivities for size III, frequency-doubling, and Gabor stimuli, and the results are shown in Figures 7 and 8. Figure 7 shows effect of ganglion cell loss on perimetric sensitivity. The examples are for D5 cortical filters with 1 octave spatial bandwidth and 54° half-height orientation bandwidth. Different symbols show simulation results for different ganglion cell arrays and D5 filters of various peak spatial frequencies. The gray line with a slope of 1 represents linearity (i.e., perimetric loss equals ganglion cell loss); points above the line represent redundancy (i.e., perimetric loss is milder than ganglion cell loss); points below the line represent cases in which perimetric loss is more severe than ganglion cell loss. Simulation with D1 and D6 filters gave similar results and data are not shown.

For FDT and Gabor stimuli, perimetric sensitivities of model simulations were primarily dependent on cortical filter peak spatial frequency, and the range of appropriate peak spatial frequencies was mainly determined by the stimulus spatial frequency. Other parameters had relatively minor impact on the results. When the peak spatial frequency of cortical filters was appropriate for the stimulus, the perimetric sensitivity versus ganglion cell loss function closely followed linearity until ganglion cell loss was >90% (1.0 log unit relative density); when the peak spatial frequency was too high, each filter responded to only a portion of the stimulus, and a filter that sampled a small patch of surviving ganglion cells could still have near-normal sensitivity, whereas most filters that sampled other portions of the ganglion cell array would have lower sensitivities. This would produce redundancy. The spacing of the ganglion cells has little effect on the results because the FDT and

Gabor stimuli are large compared with the ganglion cell spacing; therefore, only simulation results with the sparse ganglion cell array are shown.

For size III stimuli, perimetric sensitivities of model simulations were primarily dependent on ganglion cell spacing and cortical filter peak spatial frequency, and the range of appropriate peak spatial frequencies was directly related to the ganglion cell spacing; for the macular array, even 4.0 cpd was appropriate, for the dense array, 4.0 cpd was too high, and for the sparse array, 2.0 cpd was too high. Similar to FDT and Gabor stimuli, other parameters had relatively minor impact on the results.

Figure 8 illustrates possible extremes for differences in sensitivities to size III and FDT stimuli. When sensitivities for both stimuli are mediated by filters with appropriate peak spatial frequencies, sensitivity loss can be approximated by ganglion cell loss and the perimetric loss is similar for both stimuli (filled circles). When sensitivity to one stimulus is mediated by inappropriate filters while sensitivity to the other stimulus is mediated by appropriate filters, the sensitivity loss is different for the two stimuli and the difference varies with the mean (triangles).

DISCUSSION

In this study, we compared perimetric sensitivities for conventional (Goldmann size III) and sinusoidal (frequency-doubling and Gabor) stimuli using both empiric and theoretical approaches. Our data are consistent with the hypothesis that, in the macula, a linear relation between ganglion cell loss and perimetric sensitivity loss holds for all three stimuli; hence, the average perimetric loss is similar for all stimuli. This relation breaks down for advanced stages of glaucoma, in which perimetric loss tends to be greater for size III stimuli than for sinusoidal stimuli. Our data do not support the hypothesis that redundancy for frequency-doubling stimuli is

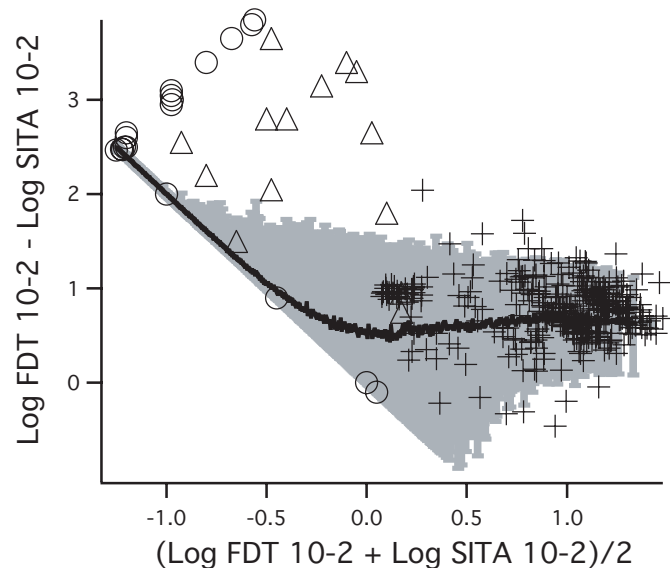


FIGURE 9.

Monte Carlo simulations of the effects of different machine range and test–retest variation on Bland-Altman analysis. The solid line shows the mean of the Monte Carlo simulation and the gray area shows the 95% confidence limits. Different symbols represent data replotted from Figure 5A.

less than redundancy for size III stimuli. In fact, for patients with severe field loss, sinusoidal stimuli may allow assessment of sensitivity at locations where size III can no longer be seen. Swanson et al.¹² have previously suggested that a linear relation between perimetric loss and ganglion cell loss holds for size III stimuli at eccentricities $>14^\circ$. The current study showed that the linearity can also be obtained in the macula although the macula is served by spatial filters tuned to higher peak spatial frequencies than in the periphery.³⁰

Artes et al.³ recently compared sensitivities (in machine units as well as in units of log contrast sensitivity) for size III and frequency-doubling stimuli in the central $\pm 30^\circ$ of visual field using principle curve analysis. They found a linear relation between frequency-doubling and size III sensitivities with a slope of 2.0 when sensitivity to size III was >25 dB. The 25 dB on the Humphrey Field Analyzer printout corresponds to the 0.0 log unit in Weber contrast sensitivity used here. When we restricted our analysis to data points with mean sensitivity of at least 0.0 log unit, we found that the difference in sensitivities was independent of mean sensitivity, which is consistent with the slope of 2.0 from Artes et al.'s study.

To further understand the effect of different machine ranges and test–retest variation on the Bland-Altman analysis, and to evaluate whether the 0.0 log contrast sensitivity boundary we set in the primary Bland-Altman analysis is appropriate, we simulated SITA 10-2 and FDT 10-2 tests for sensitivity loss ranging from 0.0 to 3.0 log units (0% to 99% ganglion cell loss) using Monte Carlo simulations. The perimetric sensitivity estimate for each location was randomly drawn from a Gaussian distribution. The mean of the Gaussian distribution was given by the normal mean and the level of sensitivity loss. For the FDT 10-2 test, the standard deviation of the Gaussian distribution was set to 0.17 log unit based on the estimate from Figure 5C, whereas for the SITA 10-2 test, the standard deviation was derived from the equation by Henson et al.³¹ for test–retest variability versus perimetric sensitivity for size III stimuli. Figure 9 shows the mean (solid line) and 95% confidence interval (gray area) of the Monte Carlo simulations for the SITA 10-2 and FDT 10-2 Bland-Altman comparison. Our data from Figure 5A are replotted here for comparison. The mean of the Monte Carlo simulations showed a similar trend as our data; it remained constant when the mean sensitivity was higher than 0.0 log unit but started to increase when the mean sensitivity was lower than 0.0 log unit. However, when the mean sensitivity was lower than 0.0 log unit, most of our data fell above the confidence limit of the Monte Carlo simulations. This indicates that the FDT 10-2 sensitivity was usually higher than the SITA 10-2 sensitivity, and this difference cannot be explained by difference in sensitivity and/or test–retest variation.

The implementation of the neural model has an implicit assumption that contrast gain of ganglion cells is linear. However, magnocellular ganglion cells show response saturation at high contrasts where response amplitude stops increasing with contrast. The response saturation might cause loss of perimetric sensitivity to be greater than loss of ganglion cells for certain conditions. As a control, we simulated perimetric sensitivity with the response saturation added to the model. The results showed that, at advanced stages of ganglion cell loss, response saturation can cause greater perimetric sensitivity loss than ganglion cell loss. If magnocellular ganglion cells contribute to the detection of size III stimuli, this

could explain the greater perimetric loss for size III stimuli than for FDT stimuli when the mean sensitivities are <0.0 log unit, because for these data points, the stimulus contrast for size III stimuli is above 2000% Weber contrast and magnocellular ganglion cell responses are likely to be saturated.

Perimetric sensitivity was on average greater for the sinusoidal stimuli than for the size III stimulus by 0.8 log unit for the grating and by 0.3 log unit for the Gabor. Both spatial and temporal factors may contribute to this difference. The model only addresses spatial factors, which determine both the relative sensitivities of filters and the relative number of filters contributing to detection. Circular stimuli can fill only a portion of the excitatory receptive field of a filter or fall on both excitatory and inhibitory portions. By comparison, sinusoidal stimuli with the appropriate orientation and peak spatial frequency can fill most of the excitatory region with luminance increments and most of the inhibitory region with luminance decrements, producing a much stronger response than for size III stimuli. Furthermore, sinusoidal stimuli cover a larger spatial area than size III stimuli, so filters at a larger number of locations will contribute to detection. However, sinusoidal stimuli have most of their energy at specific orientations and spatial frequencies, whereas circular size III stimuli have their energy distributed equally across all orientations and across a wide range of spatial frequencies, so size III stimuli will stimulate filters of a wider range of orientation angles and peak spatial frequencies. Therefore, the precise effect of spatial factors on perimetric sensitivity to sinusoids and size III stimuli will vary with the parameters of the model. To approximate the expected effect of spatial factors, we modeled a sparse mosaic sampled by weakly oriented D5 filters tuned to orientations from 0° to 330° in steps of 30° . For 1.0-cpd filters, sensitivity was predicted to be 0.6 log unit greater for the 1.0-cpd Gabor patterns than for size III. For 0.5-cpd filters, sensitivity was predicted to be 0.9 log unit greater for the 0.5-cpd grating than for size III. These values indicate that spatial factors may account for some of the difference in sensitivity.

APPENDIX

In this article, we defined sensitivity as the reciprocal of Weber's contrast,

$$\log(S_{\text{Weber}}) = -\log\left(\frac{\Delta L}{L_B}\right) \quad (1)$$

where ΔL is the luminance increment (or decrement) of the stimulus and L_B is the background luminance.

For a sinusoidal grating, Michelson contrast equals Weber's contrast.

$$\log(S_{\text{Michelson}}) = -\log\left(\frac{L_{\text{max}} - L_{\text{min}}}{L_{\text{max}} + L_{\text{min}}}\right) = -\log\left(\frac{2(L_{\text{max}} - L_{\text{mean}})}{2L_{\text{mean}}}\right) = -\log\left(\frac{\Delta L}{L_B}\right) = \log(S_{\text{Weber}}) \quad (2)$$

where L_{max} and L_{min} are the maximal and minimal luminance of the grating, respectively. L_{mean} is the mean luminance of the grating, which also equals the background luminance L_B .

In the next paragraphs, we start with the definition of sensitivities in each testing station and show how to convert them to the reciprocals of Weber's contrast.

For the Humphrey Field Analyzer, field sensitivity HFV is expressed as the retinal sensitivity in decibel units (10 dB per log unit), with 0 dB referring to maximum stimulus luminance and 51 dB referring to the minimum stimulus luminance.

$$\text{HFV} = 10\log\left(\frac{L_{\text{max}}}{\Delta L}\right) = -10\log\left(\frac{\Delta L}{L_B}\right) - 10\log\left(\frac{L_B}{L_{\text{max}}}\right) \approx 10\log(S_{\text{Weber}}) + 25 \quad (3)$$

where ΔL , L_B , and L_{max} are the luminance of the stimulus, background, and the maximal stimulus luminance, respectively.

For the Humphrey Matrix, field sensitivity HM is expressed as the reciprocal of Michelson contrast in decibel units (20 dB per log unit), with 0 dB referring to 100% contrast and 40 dB to 1% contrast.

$$\text{HM} = -20\log\left(\frac{L_{\text{max}} - L_{\text{min}}}{L_{\text{max}} + L_{\text{min}}}\right) = -20\log\left(\frac{2\Delta L}{2L_{\text{mean}}}\right) = -20\log\left(\frac{\Delta L}{L_{\text{mean}}}\right) = 20\log(S_{\text{Weber}}) \quad (4)$$

where L_{max} and L_{min} are the maximal and minimal luminance of the grating, respectively. L_{mean} is the average luminance of the grating, which also equals the background luminance L_B .

For the CRT system, the contrast of a Gabor stimulus varies as a result of its Gaussian envelope. Peli³² showed that a Gabor's apparent contrast can be estimated by the contrast of its grating component. Therefore, the threshold sensitivity is expressed as $S_{\text{Michelson}}$ of the grating component, which also equals S_{Weber} .

ACKNOWLEDGMENTS

This study was supported by NEI grant EY 007716 to WHS and the Glaucoma Institute of SUNY State College of Optometry.

Received June 24, 2005; accepted March 14, 2006.

REFERENCES

- Heijl A, Lindgren A, Lindgren G. Test-retest variability in glaucomatous visual fields. *Am J Ophthalmol* 1989;108:130-5.
- Piltz JR, Starita RJ. Test-retest variability in glaucomatous visual fields. *Am J Ophthalmol* 1990;109:109-11.
- Artes PH, Hutchison DM, Nicoletta MT, LeBlanc RP, Chauhan BC. Threshold and variability properties of matrix frequency-doubling technology and standard automated perimetry in glaucoma. *Invest Ophthalmol Vis Sci* 2005;46:2451-7.
- Wall M, Kardon R, Moore P. Effects of stimulus size on test-retest variability. In: Mills R, Heijl A, eds. *Perimetry Update 1990/91*. Amsterdam: Kugler; 1993: 371-6.
- Wall M, Kutzko KE, Chauhan BC. Variability in patients with glaucomatous visual field damage is reduced using size V stimuli. *Invest Ophthalmol Vis Sci* 1997;38:426-35.
- Wilensky JT, Mermelstein JR, Siegel HG. The use of different-sized stimuli in automated perimetry. *Am J Ophthalmol* 1986;101:710-3.
- Fellman RL, Lynn JR, Starita RJ, Swanson WH. Clinical importance of spatial summation in glaucoma. In: Heijl A, Swanson WH, eds. *Perimetry Update, 1988-89: Proceedings of the VIIIth International Perimetric Society Meeting; Vancouver, Canada; May 9-12, 1988*. Berkeley: Kugler and Ghedini; 1989:313-24.
- Chauhan BC, Johnson CA. Test-retest variability of frequency-doubling perimetry and conventional perimetry in glaucoma patients and normal subjects. *Invest Ophthalmol Vis Sci* 1999;40:648-56.

9. Spry PG, Johnson CA, McKendrick AM, Turpin A. Variability components of standard automated perimetry and frequency-doubling technology perimetry. *Invest Ophthalmol Vis Sci* 2001;42:1404–10.
10. Harwerth RS, Crawford ML, Frishman LJ, Viswanathan S, Smith 3rd, EL Carter-Dawson L. Visual field defects and neural losses from experimental glaucoma. *Prog Retin Eye Res* 2002;21:91–125.
11. Wall M, Neahring RK, Woodward KR. Sensitivity and specificity of frequency doubling perimetry in neuro-ophthalmic disorders: a comparison with conventional automated perimetry. *Invest Ophthalmol Vis Sci* 2002;43:1277–83.
12. Swanson WH, Feliuss J, Pan F. Perimetric defects and ganglion cell damage: interpreting linear relations using a two-stage neural model. *Invest Ophthalmol Vis Sci* 2004;45:466–72.
13. White AJ, Sun H, Swanson WH, Lee BB. An examination of physiological mechanisms underlying the frequency-doubling illusion. *Invest Ophthalmol Vis Sci* 2002;43:3590–9.
14. Bengtsson B, Olsson J, Heijl A, Rootzen H. A new generation of algorithms for computerized threshold perimetry, SITA. *Acta Ophthalmol Scand* 1997;75:368–75.
15. King-Smith PE, Grigsby SS, Vingrys AJ, Benes SC, Supowit A. Efficient and unbiased modifications of the QUEST threshold method: theory, simulations, experimental evaluation and practical implementation. *Vision Res* 1994;34:885–912.
16. Bland JM, Altman DG. Statistical methods for assessing agreement between two methods of clinical measurement. *Lancet* 1986;1:307–10.
17. Hood DC, Greenstein VC, Odel JG, Zhang X, Ritch R, Liebmann JM, Hong JE, Chen CS, Thienprasiddhi P. Visual field defects and multifocal visual evoked potentials: evidence of a linear relationship. *Arch Ophthalmol* 2002;120:1672–81.
18. Garway-Heath DF, Holder GE, Fitzke FW, Hitchings RA. Relationship between electrophysiological, psychophysical, and anatomical measurements in glaucoma. *Invest Ophthalmol Vis Sci* 2002;43:2213–20.
19. Reus NJ, Lemij HG. Relationships between standard automated perimetry, HRT confocal scanning laser ophthalmoscopy, and GDx VCC scanning laser polarimetry. *Invest Ophthalmol Vis Sci* 2005;46:4182–8.
20. Schlottmann PG, De Cilla S, Greenfield DS, Caprioli J, Garway-Heath DF. Relationship between visual field sensitivity and retinal nerve fiber layer thickness as measured by scanning laser polarimetry. *Invest Ophthalmol Vis Sci* 2004;45:1823–9.
21. Shadlen MN, Newsome WT. The variable discharge of cortical neurons: implications for connectivity, computation, and information coding. *J Neurosci* 1998;18:3870–96.
22. Kara P, Reinagel P, Reid RC. Low response variability in simultaneously recorded retinal, thalamic, and cortical neurons. *Neuron* 2000;27:635–46.
23. Pelli DG. Uncertainty explains many aspects of visual contrast detection and discrimination. *J Opt Soc Am (A)* 1985;2:1508–32.
24. Quick RF Jr. A vector-magnitude model of contrast detection. *Kybernetik* 1974;16:65–7.
25. Robson JG, Graham N. Probability summation and regional variation in contrast sensitivity across the visual field. *Vision Res* 1981;21:409–18.
26. Graham N, Robson JG, Nachmias J. Grating summation in fovea and periphery. *Vision Res* 1978;18:815–25.
27. Meese TS, Williams CB. Probability summation for multiple patches of luminance modulation. *Vision Res* 2000;40:2101–13.
28. Croner LJ, Kaplan E. Receptive fields of P and M ganglion cells across the primate retina. *Vision Res* 1995;35:7–24.
29. Sjostrand J, Olsson V, Popovic Z, Conradi N. Quantitative estimations of foveal and extra-foveal retinal circuitry in humans. *Vision Res* 1999;39:2987–98.
30. Olzak L, Thomas J. Seeing spatial patterns. In: Boff KR, Kaufmann L, Thomas JP, eds. *Handbook of Perception and Human Performance*, vol 1. New York: Wiley; 1986:1–56.
31. Henson DB, Chaudry S, Artes PH, Faragher EB, Ansons A. Response variability in the visual field: comparison of optic neuritis, glaucoma, ocular hypertension, and normal eyes. *Invest Ophthalmol Vis Sci* 2000;41:417–21.
32. Peli E. In search of a contrast metric: matching the perceived contrast of Gabor patches at different phases and bandwidths. *Vision Res* 1997;37:3217–24.

Hao Sun

*SUNY State College of Optometry
33 West 42nd Street
New York, NY 10036
e-mail: hsun@sunyopt.edu*